Optical properties of random alloys: A formulation

Kamal Krishna Saha* and Abhijit Mookerjee
S. N. Bose National Centre for Basic Sciences, Block-JD, Sector-III, Salt Lake City, Kolkata-700098, India
(Received 19 March 2004; revised manuscript received 7 June 2004; published 18 October 2004)

We present here a formulation for the calculation of the configuration-averaged optical conductivity in random alloys. Our formulation is based on the augmented-space theorem introduced by one of us [A. Mookerjee, J. Phys. C **6**, 1340 (1973)]. We show that disorder scattering renormalizes the electron and hole propagators as well as the transition amplitude. The corrections to the transition amplitude have been shown to be related to the self-energy of the propagators and vertex corrections.

DOI: 10.1103/PhysRevB.70.134205 PACS number(s): 71.23.−k

I. INTRODUCTION

The object of our present study is to present a formulation for obtaining the configuration-averaged optical conductivity for random alloys. Because of randomness, there is a need to go beyond the usual reciprocal-space-based formulations for crystalline compounds. Instead of labeling the electronic states by the Bloch wave vector and band index $(\mathbf{k},j)$, which is suitable for crystalline compounds, we have to label them by energy and the composite angular momentum $L=(\ell,m,m_s)$. In cases where the disorder is substitutional and *homogeneous*, in the sense that the occupation probabilities of lattice sites by atom species are independent of the site label, we can still label the configuration-averaged quantities by the reciprocal wave vectors. However, the band picture breaks down, and we cannot use the band index labeling of quantum states as in crystalline materials. Substitutional disorder dictates that we begin with a purely real-space representation, and we have chosen the minimal basis set of the tight-binding linear muffin-tin orbitals (TB-LMTO) method.[1,2] Configuration averaging over various random atomic arrangements has been carried out using the augmented-space formalism (ASF) introduced by us earlier for the study of electronic properties of disordered systems.[3,7] The ASF goes beyond the usual mean-field approaches and takes into account configuration fluctuations. This formalism has been described in detail in the referenced articles and the interested reader can go into the details in them. The contribution of the paper will be to show that the disorder-induced corrections to the averaged current terms in the optical conductivity are directly related either to the disorder-induced self-energy in the propagators or to vertex corrections. Since the self-energy and the vertex corrections can be calculated for realistic binary alloy systems, either within an augmented-space recursion[5–7] or within one of the mean-field approaches,[4] this formulation will form the basis of subsequent calculations in real alloys.

II. THE OPTICAL CONDUCTIVITY

The Hamiltonian describing the effect of an external radiation field on the electronic states of a solid is given by

$$H=\sum_{i=1}^{N}\left\{\frac{1}{2}[\mathbf{p}_i+\mathbf{A}(\mathbf{r}_i,t)]^2+V(\mathbf{r}_i)+\phi(\mathbf{r}_i,t)\right\}.$$

Here $\mathbf{A}(\mathbf{r}_i,t)$ and $\phi(\mathbf{r}_i,t)$ are the vector and scalar potentials seen by the ith electron because of the radiation field. We have used atomic units in which the electronic charge, mass, the Planck constant, and the velocity of light are set to unity ($e=1$, $m=1$, $\hbar=1$, $c=1$). There are N electrons whose positions are labeled by $\mathbf{r}_i$. The effective potential $V(\mathbf{r}_i)$ experienced by individual electrons is expressed in the local-density approximation (LDA) of the density-functional theory (DFT). To first order in the vector potential, the Hamiltonian becomes

$$H=\sum_{i=1}^{N}\left\{\frac{1}{2}\mathbf{p}_i^2+V(\mathbf{r}_i)+\mathbf{A}(\mathbf{r}_i,t)\cdot\mathbf{j}_i\right\}. \tag{1}$$

The current operator $\mathbf{j}_i$ is related to the momentum operator as $(e/m)\mathbf{p}_i$. In atomic units, $\mathbf{j}_i=\mathbf{p}_i=\mathbf{v}_i=d\mathbf{r}_i/dt$. We work in the Coulomb gauge where $\nabla\cdot\mathbf{A}(\mathbf{r}_i,t)=0$ and $\phi(\mathbf{r}_i,t)=0$, so that the electric field

$$\mathbf{E}(\mathbf{r}_i,t)=-\frac{\partial\mathbf{A}(\mathbf{r}_i,t)}{\partial t}.$$

The Kubo formula relates the linear current response to the radiation field,

$$\langle j_\mu(t)\rangle=\sum_{\upsilon}\int_{-\infty}^{\infty}dt'\chi_{\mu\nu}(t-t')A_\nu(t'),$$

$$\chi_{\mu\nu}(\tau)=\imath\Theta(\tau)\langle\Phi_0|[j_\mu(\tau),j_\nu(0)]|\Phi_0\rangle,$$

where $\tau=t-t'$ and $\Theta(\tau)$ is the Heaviside step function,

$$\Theta(\tau)=\begin{cases}1 & \text{if} \quad \tau>0\\ 0 & \text{if} \quad \tau\leqslant 0.\end{cases}$$

$|\Phi_0\rangle$ is the ground state of the unperturbed system, that is, the electrons in the solid in the absence of the radiation field. In the absence of the radiation field, there is no photocurrent, i.e., $\langle\Phi_0|j_\mu|\Phi_0\rangle=0$. The fluctuation-dissipation theorem relates the imaginary part of the generalized susceptibility to the correlation function as follows:

$$\chi''_{\mu\nu}(\omega) = \frac{1}{2}(1 - e^{-\beta\omega})S_{\mu\nu}(\omega), \tag{2}$$

where $\beta = 1/k_B T$; k_B is the Boltzmann constant, T is the temperature, and

$$\chi''_{\mu\nu}(\omega) = \mathrm{Im}\int_{-\infty}^{\infty} dt\ e^{\imath z\tau}\chi_{\mu\nu}(\tau), \quad z = \omega + \imath 0^+$$

and

$$S_{\mu\nu}(\omega) = \mathrm{Im}\int_{-\infty}^{\infty} dt\ e^{\imath z\tau}\langle\Phi_0|j_\mu(\tau)j_\nu(0)|\Phi_0\rangle, \quad z = \omega + \imath 0^+.$$

An expression for the correlation function, at $T=0$ K, can be obtained via the Kubo-Greenwood expression,

$$S(\omega) = \frac{1}{3\pi}\sum_\gamma \int dE\ \mathrm{Tr}[\mathbf{j}_\gamma\ \mathrm{Im}\{\mathbf{G}^v(E)\}\mathbf{j}_\gamma^\dagger \mathrm{Im}\{\ \mathbf{G}^c(E+\omega)\}]. \tag{3}$$

We have assumed isotropy of the response so that the tensor $S_{\mu\nu}$ is diagonal and we have defined $S(\omega)$ as the direction averaged quantity $\frac{1}{3}\Sigma_\mu\ S_{\mu\mu}(\omega)$. $\mathbf{j}_\gamma$ is $\hat{e}_\gamma\cdot\mathbf{j}$, and $\hat{e}_\gamma$ is the direction of polarization of the incoming photon. The operators $\mathbf{G}^v(E)$ and $\mathbf{G}^c(E)$ are the resolvents of the Hamiltonian projected onto the subspaces spanned by the occupied and the unoccupied one-electron states.

The trace is invariant in different representations. For crystalline systems, usually the Bloch basis $\{|\mathbf{k},j\rangle\}$ is used. For disordered systems, prior to configuration averaging, it is more convenient to use the real-space-based screened (or tight-binding) muffin-tin orbitals as a basis $\{|RL\rangle\}$.

If we define

$$\mathcal{S}_\gamma(z_1,z_2) = \mathrm{Tr}[\mathbf{j}_\gamma\mathbf{G}^v(z_1)\mathbf{j}_\gamma^\dagger\mathbf{G}^c(z_2)], \tag{4}$$

then the above equation becomes

$$S(\omega) = \frac{1}{12\pi}\sum_\gamma \int dE[\mathcal{S}_\gamma(E^-,E^+ + \omega) + \mathcal{S}_\gamma(E^+,E^- + \omega) - \mathcal{S}_\gamma(E^+,E^+ + \omega) - \mathcal{S}_\gamma(E^-,E^- + \omega)], \tag{5}$$

where

$$f(E^\pm) = \lim_{\delta\to 0} f(E \pm i\delta).$$

We have used the Herglotz property of the Green operator,

$$\mathbf{G}(E + i\delta) = \mathbf{G}^r(E) - i\ \mathrm{sgn}(\delta)\mathbf{G}^i(E).$$

For disordered materials, we shall be interested in obtaining the configuration-averaged response functions. This will require the configuration averaging of quantities such as $\mathcal{S}_\gamma(z_1,z_2)$.

III. CONFIGURATION AVERAGING

Any description of a disordered system must be from a statistical point of view, since the properties of these systems are random variables and any particular *configuration* is of little interest.[31] Consequently, the study of configuration-averaged properties of disordered systems has received much attention.

Configuration averaging for response functions in disordered materials has had some history. The Ziman-Faber theory,[8–10] much in use for liquids, is valid for electrons, weakly scattered from a dilute distribution of impurities. The extended version of this theory was proposed by Evans *et al.*,[11] but this too overlooks multiple scattering effects, as pointed out by Roth and Singh.[12] An effective-medium approach (EMA) was proposed by Roth[13] and developed further by Roth and Singh[12–14] and Asano and Yonezawa.[15] This approach does take into account multiple scattering effectively and, as we shall see, will have close similarities with the approach we propose in this paper. Velický[16] has developed an expression for configuration-averaged response functions in random alloys for simple tight-binding models with one orbital per site and diagonal disordered within the coherent-potential approximation (CPA). Brouers and Vedyayev[17] have extended the formalism to transition–noble metal alloys. The CPA-like mean-field approach has been applied to response functions by Niizeki and co-workers,[18–20] who extended the pioneering work of Velický[16] to longer-ranged random potentials. Mookerjee[3] has introduced the ASF to tackle configuration averaging. Within this formalism, he studied the role of macroscopic conservation laws on the response functions, leading to a Ward identity between the vertex corrections and the self-energy.[21] Within the CPA, vertex corrections were obtained by ingenious diagram summations by Leath.[22] There have been CPA calculations by Harris and Plischke[23] and Nauciel-Bloch and Riedinger.[24] In a series of papers, Mookerjee and co-workers[25–27] have applied the ASF to conductivity and optical conductivity in random alloys. This will form the background of our present development.

The ASF has been described thoroughly in a series of articles.[3–7] Here we shall introduce the salient features which will be required by us subsequently in this paper. We shall start from a first-principles tight-binding linear muffin-tin orbitals (TB-LMTO) method.[1,2]

The quenched local randomness in the alloy is described by a set of random *occupation* variables n_R, which takes the value 1 if the muffin-tin labeled by $\{R\}$ is occupied by an A-type atom and 0 if it is occupied by a B. The atom sitting at $\{R\}$ can either be of the type A ($n_R=1$) with probability x_A or B ($n_R=0$) with probability x_B.

The ASF now introduces the configuration space Φ of the set of N random variables $\{n_R\}$ of rank 2^N spanned by configurations of the kind $|\uparrow\uparrow\downarrow\cdots\downarrow\uparrow\cdots\rangle$, where

$$|\uparrow_R\rangle = \sqrt{x_A}|A_R\rangle + \sqrt{x_B}|B_R\rangle,$$

$$|\downarrow_R\rangle = \sqrt{x_B}|A_R\rangle - \sqrt{x_A}|B_R\rangle.$$

If we define the configuration $|\uparrow\uparrow\cdots\uparrow\cdots\rangle$ as the *average* or *reference* configuration, then any other configuration may be uniquely labeled by the *cardinality sequence*, $\{R_k\}$, which is the sequence of positions where we have a $\downarrow$ configuration.

The *cardinality sequence* of the *reference* configuration is the null sequence $\{\varnothing\}$.

The augmented-space theorem[3] states that

$$\langle\langle A(\{n_R\})\rangle\rangle = \langle\{\varnothing\}|\tilde{\mathbf{A}}|\{\varnothing\}\rangle, \tag{6}$$

where

$$\tilde{\mathbf{A}}(\{\mathbf{M}_R\}) = \int \cdots \int A(\{\lambda_R\}) \prod d\mathbf{P}(\lambda_R)\ \epsilon\ \Phi.$$

$\mathbf{P}(\lambda_R)$ is the spectral density of the self-adjoint operator $\mathbf{M}_R$, which is such that the probability density of n_R is given by

$$p(n_R) = -\frac{1}{\pi}\lim_{\delta\to 0} \mathrm{Im}\langle\uparrow|[(n_R + i\delta)\mathbf{I} - \mathbf{M}_R]^{-1}|\uparrow\rangle.$$

$\mathbf{M}_R$ is an operator in the space of configurations ψ_R of the variable n_R. This is of rank 2 and is spanned by the *states* $\{|\uparrow_R\rangle, |\downarrow_R\rangle\}$,

$$\mathbf{M}_R = x_A\mathcal{P}_R^{\uparrow} + x_B\mathcal{P}_R^{\downarrow} + \sqrt{x_A x_B}(\mathcal{T}_R^{\uparrow\downarrow} + \mathcal{T}_R^{\downarrow\uparrow}), \tag{7}$$

where $\mathcal{P}_R^{\uparrow} = |\uparrow_R\rangle\langle\uparrow_R|$, $\mathcal{P}_R^{\downarrow} = |\downarrow_R\rangle\langle\downarrow_R|$, and $\mathcal{T}_R^{\uparrow\downarrow} = |\uparrow_R\rangle\langle\downarrow_R|$, are projection and transfer operators in configuration space.

Within the ASF, the configuration-averaged Green function is given by[29]

$$\langle\langle \mathbf{G}(z)\rangle\rangle = \langle 1|(z\tilde{\mathbf{I}} - \tilde{\mathbf{H}}^{\mathrm{eff}})^{-1}|1\rangle. \tag{8}$$

$$\tilde{\mathbf{H}}^{\mathrm{eff}} = \sum_R \left\{ \tilde{\mathbf{A}}\mathcal{P}_R \otimes \tilde{\mathcal{I}} + \tilde{\mathbf{B}}\mathcal{P}_R \otimes \mathcal{P}_R^{\downarrow} + \tilde{\mathbf{F}}\mathcal{P}_R \otimes (\mathcal{T}_R^{\uparrow\downarrow} + \mathcal{T}_R^{\downarrow\uparrow}) + \sum_{R'} \tilde{\mathbf{V}}_{RR'}\mathcal{T}_{RR'} \otimes \tilde{\mathcal{I}} \right\}, \tag{9}$$

where

$$\tilde{\mathbf{A}} \equiv \tilde{A}_L\delta_{LL'} = A(C_L/\Delta_L)/A(1/\Delta_L)\delta_{LL'},$$

$$\tilde{\mathbf{B}} \equiv \tilde{B}_L\delta_{LL'} = B[(C_L - z)/\Delta_L]/A(1/\Delta_L)\delta_{LL'},$$

$$\tilde{\mathbf{F}} \equiv \tilde{F}_L\delta_{LL'} = F[(C_L - z)/\Delta_L]/A(1/\Delta_L)\delta_{LL'},$$

$$\tilde{\mathbf{V}} \equiv \tilde{V}_{LL'}(R - R') = A(1/\Delta_L)^{-1/2}S_{LL'}(R - R')A(1/\Delta_{L'})^{-1/2}. \tag{10}$$

$\mathcal{P}_R = |R\rangle\langle R|$ and $\mathcal{T}_{RR'} = |R\rangle\langle R'|$ are projection and transfer operators in real space, and L is a composite angular momentum index $\{\ell, m, m_s\}$. C, Δ are the TB-LMTO potential parameters and S is the structure matrix, in the most tight-binding (α) representation.[1,2] The following functions are

$$A(y) = x_A y_A + x_B y_B, \quad \text{i.e., the average of } y,$$

$$B(y) = (x_B - x_A)(y_A - y_B),$$

$$F(y) = \sqrt{x_B x_A}(y_A - y_B),$$

and

$$|1\} = A(\Delta_L^{-1/2})|\{\varnothing\}\rangle + F(\Delta_L^{-1/2})|\{R\}\rangle, \quad |1\rangle = \frac{|1\}}{\||1\}\|}.$$

We can reformulate the above in a second quantized formalism. This follows the ideas put forward by Schultz and Shapero,[28] which were extended in the ASF by Mookerjee.[25] For the real-space part, this is straightforward, with a *vacuum* state described as that one which contains no electron-like excitations, and the fermion creation and annihilation operators are $a_{RL}^{\dagger}$ and a_{RL} for electrons at the site R with angular momentum indices L. For the configuration-space part, we shall follow the ideas of Ref. 28 and consider the *reference* state to be the vacuum. Each *spin flip*[32] at any site from up to down is then a creation of a configuration fluctuation. Since each site can have only two configurations, two up to down *spin flips* cannot take place at a site. These excitations are then *local* and *fermion-like*. Each spin flip from down to up is a destruction of such a *local pseudo-fermion*. The Fock space is then spanned by all configuration states labeled by the cardinality sequences. The corresponding fermion-like creation and annihilation operators are $b_R^{\dagger}$ and b_R. These create and annihilate configuration fluctuations over the reference state. We should note that the configuration fluctuations are local and quenched. In second-quantized form, the Hamiltonian becomes

$$\tilde{\mathbf{H}} = \tilde{\mathbf{H}}_0 + \tilde{\mathbf{H}}_1,$$

$$\tilde{\mathbf{H}}_0 = \sum_{RL} \tilde{A}_L a_{RL}^{\dagger}a_{RL} + \sum_{RL}\sum_{R'L'} \tilde{V}_{RL,R'L'}a_{RL}^{\dagger}a_{R'L'},$$

$$\tilde{\mathbf{H}}_1 = \sum_{RL} \{\tilde{B}_L a_{RL}^{\dagger}a_{RL}b_R^{\dagger}b_R + \tilde{F}_L a_{RL}^{\dagger}a_{RL}(b_R + b_R^{\dagger})\}, \tag{11}$$

where

$$\{b_R, b_{R'}^{\dagger}\} = \delta_{RR'},$$

$$\{b_R, b_{R'}\} = 0 = \{b_R^{\dagger}, b_{R'}^{\dagger}\},$$

and the contraction

$$b(x')\cdot b(x)^{\dagger\cdot} = i\theta(t' - t)\delta_{RR'},$$

where

$$b(x) = b_R(t) = \exp(it\tilde{\mathbf{H}}_0)b_R \exp(-it\tilde{\mathbf{H}}_0)$$

so that

$$\gamma(x,x') = -i\langle\{\varnothing\}|\{Tb(x')b^{\dagger}(x)\}|\{\varnothing\}\rangle = -i\theta(t' - t)\delta_{RR'}\delta(t - t'). \tag{12}$$

This *pseudo-fermion* formalism has been described earlier by Mookerjee.[25] The readers are referred to that article for further details.

IV. AVERAGED GREEN FUNCTION IN THE PSEUDO-FERMION FORMALISM

In this section, we shall develop a multiple scattering formalism for the configuration-averaged Green function for a

random binary alloy. The scattering is by configuration fluctuations and within the second-quantized formalism just described, the scattering diagrams are Feynman diagrams. The formalism is very close to the Yonezawa-Matsubara scattering diagrams[15] and one can establish a one-to-one correspondence between them in the special case of diagonal disorder.

The augmented-space theorem then states that

$$\langle\langle \mathbf{G}(x,x')\rangle\rangle = -i\sum_{n=0}^{\infty}\frac{(-i)^n}{n!}\int\cdots\int dt_1 dt_2\ldots dt_n \times\frac{\langle 0|\{T\tilde{\mathbf{H}}_1(t_1)\cdots\tilde{\mathbf{H}}_n(t_n)a(x)a^{\dagger}(x')\}|0\rangle}{\langle 0|\tilde{\mathbf{S}}|0\rangle},$$

where it is understood that the boldface operators are expressed by the matrix representation in $\{L\}$ space and

$$a(x) = a_{RL}(t) = \exp(it\tilde{\mathbf{H}}_0)a_{RL}\exp(-it\tilde{\mathbf{H}}_0),$$

$$\tilde{\mathbf{S}} = \tilde{\mathbf{U}}(\infty,-\infty) \quad \text{and} \quad |0\rangle = |0\otimes\{\varnothing\}\rangle,$$

and

$$\tilde{\mathbf{U}}(t,t') = \tilde{\mathbf{I}} - \int_{-\infty}^{t} dt''\tilde{\mathbf{H}}_1(t'')\tilde{\mathbf{U}}(t'',t').$$

We may now apply Wick's theorem and Feynman's rules and generate a diagrammatic expansion for the averaged Green function $\langle\langle \mathbf{G}(x,x')\rangle\rangle$ in terms of the VCA Green function,

$$\mathbf{g}(x,x') = -i\langle 0|\{Ta(x)a^{\dagger}(x')\}|0\rangle.$$

Let us examine a few terms in the series.

(i) For $n=1$, the term in the expansion is

$$-i\int dt_1\langle 0|\{T\tilde{\mathbf{H}}_1(t_1)a(x)a^{\dagger}(x')\}|0\rangle_{\text{conn}}.$$

The contribution of this term is zero, since all three terms arising out of $\tilde{\mathbf{H}}_1$ [see Eq. (11)] vanish because $\langle\{\varnothing\}|b^{\dagger}(x)b(x)|\{\varnothing\}\rangle$, $\langle\{\varnothing\}|b^{\dagger}(x)|\{\varnothing\}\rangle$, and $\langle\{\varnothing\}|b(x)|\{\varnothing\}\rangle$ are all zero.

(ii) For $n=2$, the only nonvanishing terms come from

$$\begin{aligned} i^2\int dt_1\int dt_2\langle 0|\{T\tilde{\mathbf{H}}_1(t_1)\tilde{\mathbf{H}}_1(t_2)a(x)a^{\dagger}(x')\}|0\rangle_{\text{conn}} &= F^2\int dx_1\int dx_2\langle 0|\{Ta^{\dagger}(x_1)a(x_1)a^{\dagger}(x_2)a(x_2)a(x)a^{\dagger}(x')\} \\ &\quad\times|0\rangle_{\text{conn}}\langle\{\varnothing\}|T[b^{\dagger}(x_1)+b(x_1)][b^{\dagger}(x_2)+b(x_2)]|\{\varnothing\}\rangle_{\text{conn}} \\ &= F^2[\mathbf{g}(x,x_1)\mathbf{g}(x_1,x_2)\mathbf{g}(x_2,x')\gamma(x_1,x_2) \\ &\quad+\mathbf{g}(x,x_2)\mathbf{g}(x_2,x_1)\mathbf{g}(x_1,x')\gamma(x_2,x_1)]. \end{aligned}$$

Figure 1(a) shows a pictorial representation of the two terms, which are topologically identical and therefore have identical contributions. This cancels the $(1/2!)$ term in the expansion for $\langle\langle \mathbf{G}(x,x')\rangle\rangle$. The F vertex [see Eq. (11)] has a contribution $F_{LL'}$ which is diagonal in L space $F_{LL'}=F_L\delta_{LL'}$, where

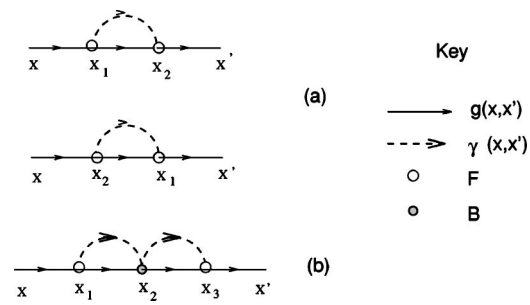

FIG. 1. The scattering diagrams for (a) the two topologically identical diagrams for $n=2$ and (b) one of the 3! topologically identical diagrams for $n=3$.

$$F_L = \sqrt{x_B x_A}\left\langle\frac{1}{\Delta_L}\right\rangle^{-1}\left[\frac{C_L^A}{\Delta_L^A}-\frac{C_L^B}{\Delta_L^B}-z\left(\frac{1}{\Delta_L^A}-\frac{1}{\Delta_L^B}\right)\right].$$

(iii) Figure 1(b) shows one of the topologically identical diagrams (there are $3!=6$ such diagrams) for $n=3$. Note that it involves the scattering vertex B. This arises from the first term in the expression for $\tilde{\mathbf{H}}_1$ in Eq. (11). Its contribution is also diagonal in L space $B_{LL'}=B_L\delta_{LL'}$ where

$$B_L = \frac{(x_B - x_A)}{\sqrt{x_B x_A}}F_L.$$

This scattering vertex cannot sit either in the leftmost or in the rightmost positions, because one of the associated pseudo-fermion propagators vanishes.

(iv) For $n=4$, there are two topologically distinct nonseparable diagrams:[33] the double tent and the crossed tent diagrams shown as the two top diagrams in Fig. 2. The inner tent in the top diagram goes on to renormalize the interior Green function from $\mathbf{g}(x,x')$ to $\langle\langle \mathbf{G}(x,x')\rangle\rangle$. As such, the middle diagram is the only *skeleton* diagram at this order. There is one separable diagram (the bottom diagram in Fig. 2). This can be broken into two, as shown, by the dotted line. The rightmost diagram renormalizes the rightmost electron line.

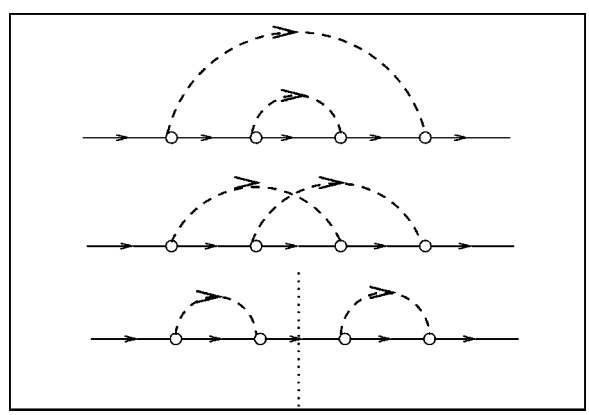

FIG. 2. The topologically distinct scattering diagrams for $n=4$. Top and middle are nonseparable, the bottom is separable. The middle diagram is a skeleton one.

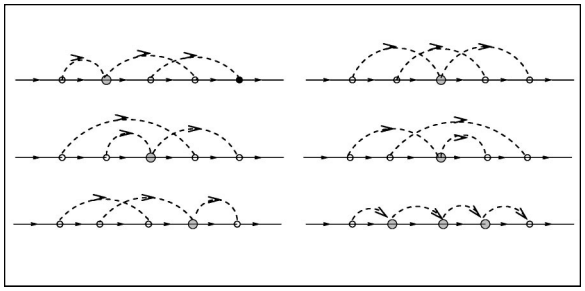

FIG. 3. Skeleton diagrams for order $n=5$.

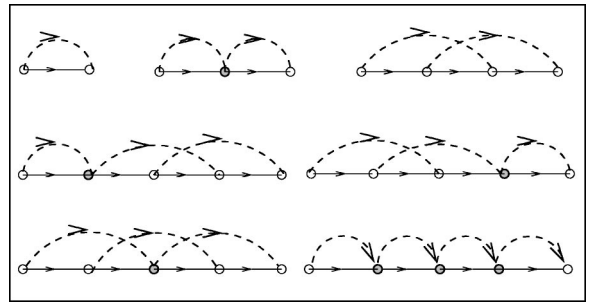

FIG. 4. The skeleton diagrams for the self-energy $\Sigma(z)$.

(v) The nonseparable topologically distinct diagrams for $n=5$ are shown in Fig. 3. We note that all odd-order diagrams must have an odd number of B vertices.

The skeleton diagrams provide the expression for the self-energy for the Dyson equation which follows:

$$\langle\langle \mathbf{G}(x,x')\rangle\rangle = \mathbf{g}(x,x') + \int dy \int dy' \mathbf{g}(x,y)\Sigma(y,y')\langle\langle \mathbf{G}(y',x')\rangle\rangle.$$

For homogeneous disorder, we have shown earlier that we have translational symmetry in the full augmented space.[29] We can then take the Fourier transform of the above equation to get

$$\mathbf{G}(\mathbf{k},E) = \mathbf{g}(\mathbf{k},E) + \mathbf{g}(\mathbf{k},E)\Sigma(\mathbf{k},E)\mathbf{G}(\mathbf{k},E). \tag{13}$$

The diagrams for the self-energy are shown in Fig. 4. In the above equation, each term is a matrix in $\{L\}$ space.

V. AVERAGED OPTICAL CONDUCTIVITY IN THE PSEUDO-FERMION FORMALISM

We now go back to Eq. (4) and discuss the configuration averaging of the two-particle Green functions of the kind $\mathcal{S}_\gamma(z_1,z_2)$. The augmented-space theorem immediately implies that

$$\langle\langle \mathcal{S}_\gamma(z_1,z_2)\rangle\rangle = \mathrm{Tr}\langle\{\varnothing\}|[\tilde{\mathbf{j}}_\gamma \tilde{\mathbf{G}}^v(z_1)\tilde{\mathbf{j}}_\gamma^\dagger \tilde{\mathbf{G}}^c(z_2)]|\{\varnothing\}\rangle. \tag{14}$$

The first thing to note about Eq. (14) is that the right-hand side is an average of four random functions whose fluctuations are correlated. The average of the product then involves the product of the averages and other contributions which come from averages taken in pairs, triplets, and all four random functions.

A. Disorder-induced renormalization of the current terms

At this stage, in order to simplify notation, we shall omit the L index. However, we have to remember that all terms labeled by indices R or $\mathbf{k}$ are matrices in $\{L\}$ space, so the order of multiplication of various terms in the expression has to be preserved. We shall also omit the γ index of the current term indicating the required projection onto a direction. If required, we can put them back in the final expression.

The real-space representation of the random current operator, can take the values $\mathbf{j}_{RR'}^{AA}$, $\mathbf{j}_{RR'}^{AB}$, $\mathbf{j}_{RR'}^{BA}$, or $\mathbf{j}_{RR'}^{BB}$ with probabilities x_A^2, x_Ax_B, x_Bx_A, and x_B^2, respectively. We may rewrite $\mathbf{j}_{RR'}$ as

$$\mathbf{j}_{RR'} = \mathbf{j}_{RR'}^{AA} n_R n_{R'} + \mathbf{j}_{RR'}^{AB} n_R(1-n_{R'}) + \mathbf{j}_{RR'}^{BA}(1-n_R)n_{R'} + \mathbf{j}_{RR'}^{BB}(1-n_R)(1-n_{R'}).$$

Following the same augmented-space procedure as for the single-particle Green functions, we get

$$\begin{aligned}\mathbf{j} = \sum_R \sum_{R'} [&\langle\langle \mathbf{j}\rangle\rangle_{RR'} a_R^\dagger a_R + (x_B - x_A)\mathbf{j}_{RR'}^{(1)} a_R^\dagger a_{R'}(b_R^\dagger b_R + b_{R'}^\dagger b_{R'}) + \sqrt{x_Ax_B}\,\mathbf{j}_{RR'}^{(1)} a_R^\dagger a_{R'}(b_R + b_R^\dagger + b_{R'}^\dagger + b_{R'}) \\ &+ (x_B - x_A)\sqrt{x_Ax_B}\,\mathbf{j}_{RR'}^{(2)} a_R^\dagger a_{R'}\{b_R^\dagger b_R(b_{R'}^\dagger + b_{R'}) + b_{R'}^\dagger b_{R'}(b_R^\dagger + b_R)\} + (x_B - x_A)^2 \mathbf{j}_{RR'}^{(2)} a_R^\dagger a_{R'} b_{R'}^\dagger b_{R'} b_R^\dagger b_R \\ &+ x_Ax_B\,\mathbf{j}_{RR'}^{(2)} a_R^\dagger a_{R'}\{(b_R^\dagger + b_R)(b_{R'}^\dagger + b_{R'})\},\end{aligned} \tag{15}$$

where

$$\mathbf{j}_{RR'}^{(1)} = x_A(\mathbf{j}_{RR'}^{AA} - \mathbf{j}_{RR'}^{AB}) - x_B(\mathbf{j}_{RR'}^{BB} - \mathbf{j}_{RR'}^{BA}),$$

$$\mathbf{j}_{RR'}^{(2)} = \mathbf{j}_{RR'}^{AA} + \mathbf{j}_{RR'}^{BB} - \mathbf{j}_{RR'}^{AB} - \mathbf{j}_{RR'}^{BA}.$$

The first term in Fig. 5 is the averaged current. The figure shows the 15 different scattering vertices arising from terms in Eq. (15). The rule for obtaining the diagrams for the cor-

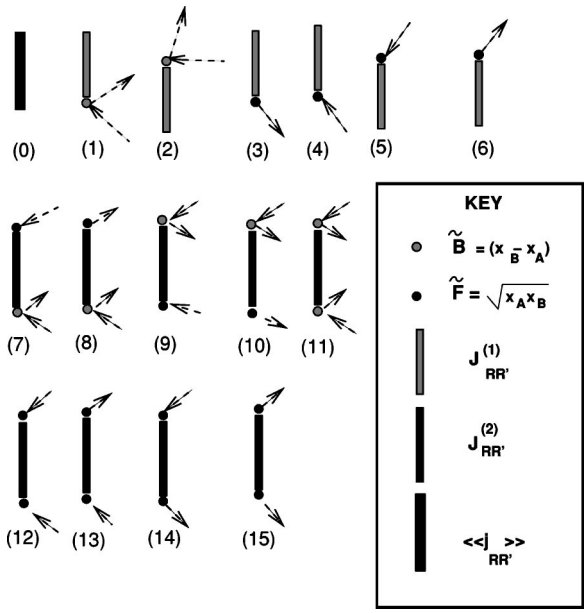

FIG. 5. The scattering vertices associated with the random current terms.

relation function $S_\gamma(z_1,z_2)$ is as follows: Take any two current diagrams from Fig. 5 and two propagators and join them end to end. Now join the configuration fluctuation lines (shown as dashed arrows) in all possible ways.

The dominant contribution comes from the diagram shown in Fig. 6. Here the two current terms are the averaged current, and all configuration-fluctuation decorations renormalize only the two electron propagators. In this diagram the bold propagators are the fully renormalized electron propagators and the contribution of this term is

$$\int_{\mathrm{BZ}} \frac{d^3\mathbf{k}}{8\pi^3} \langle\langle \mathbf{j}(\mathbf{k})\rangle\rangle \langle\langle \mathbf{G}^v(\mathbf{k},z_1)\rangle\rangle \langle\langle \mathbf{j}(\mathbf{k})\rangle\rangle^\dagger \langle\langle \mathbf{G}^c(\mathbf{k},z_2)\rangle\rangle. \quad (16)$$

We now focus on the main correction terms to the expression in Eq. (16). These are the correction terms to the averaged current which are closely related to the self-energies. They arise from a set of diagrams in which no disorder propagator (shown as dashed lines) joins either two electron propagators or two of the current lines directly. These diagrams are made out of a left *renormalized* current diagram chosen out of the diagrams (1)–(4) in Fig. 7 and one right *renormalized* current diagram from (5)–(8) connected by two *renormalized* propagators, the bottom one being a valence and the top a conduction electron propagator.

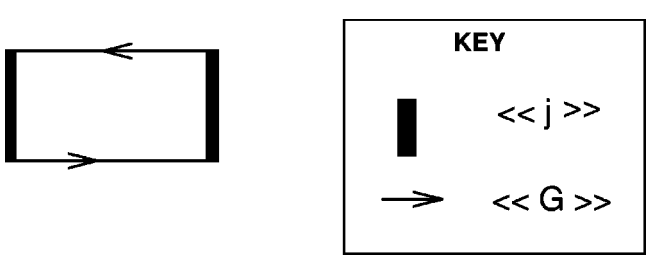

FIG. 6. The diagram for $[\langle\langle \mathbf{j}\rangle\rangle\langle\langle G^v\rangle\rangle\langle\langle \mathbf{j}\rangle\rangle\langle\langle G^c\rangle\rangle]$.

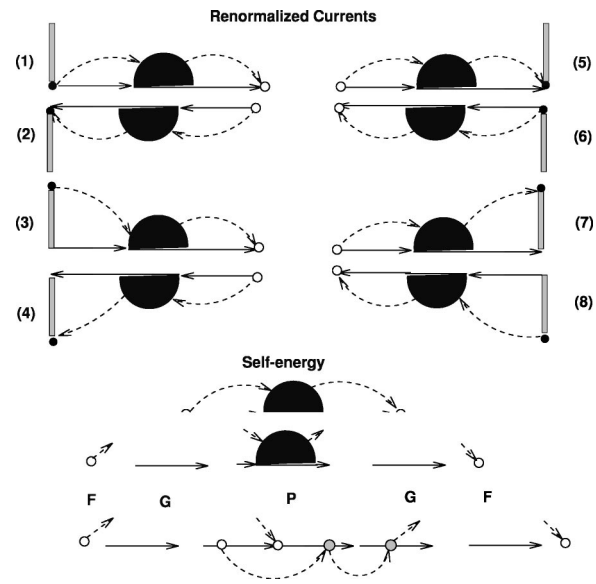

FIG. 7. Relation between the renormalized currents and the self-energy.

Let us now obtain expressions for the renormalized currents. A careful look at the self-energy diagrams (see the bottom of Fig. 7 and the example diagram shown there) shows that all self-energy diagrams have the structure

$$\mathbf{\Sigma}(\mathbf{k},z) = \mathbf{F}(z)\mathbf{\Phi}(\mathbf{k},z)\mathbf{F}(z),$$

where $\mathbf{\Phi}(\mathbf{k},z)$ is the Fourier transform of

$$\mathbf{\Phi}_{RR'}(z) = \sum_{R_1R_2} G_{RR_1}(z) P^{RR'}_{R_1R_2}(z) G_{R_2R'}(z).$$

While the contribution of the diagram labeled (1) in Fig. 7 is

$$\mathbf{j}^{(1)}(\mathbf{k})\tilde{\mathbf{F}}(z_1)\mathbf{\Phi}(\mathbf{k},z_1)\mathbf{F}(z_1), \quad (17)$$

where

$$F_{LL'}(z) = \sqrt{x_A x_B}\frac{1}{f_L(z)}\delta_{LL'},$$

$$\tilde{F}_{LL'} = \sqrt{x_A x_B}\delta_{LL'},$$

the expression for (17) becomes

$$\mathbf{j}^{(1)}(\mathbf{k})\tilde{\mathbf{F}}(z_1)\mathbf{F}^{-1}(z_1)\Sigma(\mathbf{k},z_1) = \mathbf{j}^{(1)}(\mathbf{k})\mathbf{f}(z_1)\mathbf{\Sigma}(\mathbf{k},z_1).$$

The contributions of the other diagrams in the left column of Fig. 7 are:

$$\mathbf{\Sigma}(\mathbf{k},z_2)\mathbf{F}^{-1}(z_2)\tilde{\mathbf{F}}(z_2)\mathbf{j}^{(1)}(\mathbf{k}) = \mathbf{\Sigma}(\mathbf{k},z_2)\mathbf{f}(z_2)\mathbf{j}^{(1)}(\mathbf{k}),$$

$$\tilde{\mathbf{F}}(z_1)\mathbf{j}^{(1)}(\mathbf{k})\mathbf{F}^{-1}(z_1)\mathbf{\Sigma}(\mathbf{k},z_1) = \mathbf{j}^{(1)}(\mathbf{k})\mathbf{f}(z_1)\mathbf{\Sigma}(\mathbf{k},z_1),$$

$$\mathbf{\Sigma}(\mathbf{k},z_2)\mathbf{F}^{-1}(z_2)\mathbf{j}^{(1)}(\mathbf{k})\tilde{\mathbf{F}}(z_2) = \mathbf{\Sigma}(\mathbf{k},z_2)\mathbf{f}(z_2)\mathbf{j}^{(1)}(\mathbf{k}).$$

From the forms of $\mathbf{F}(z)$ and $\tilde{\mathbf{F}}(z)$, we note that

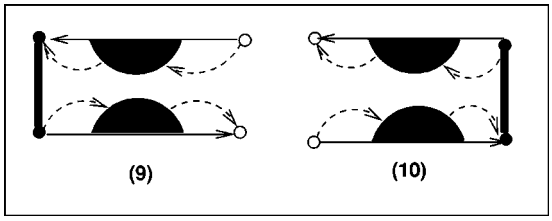

FIG. 8. Few more renormalized currents.

$$\mathbf{j}^{(1)}(\mathbf{k})\tilde{\mathbf{F}}(z)\mathbf{F}(z) = \tilde{\mathbf{F}}(z)\mathbf{j}^{(1)}(\mathbf{k})\mathbf{F}(z) = \mathbf{j}^{(1)}_{LL'}(\mathbf{k})f_{L'}(z).$$

Similarly, the contributions of the diagrams in the right column in Fig. 7 are

$$\Sigma(\mathbf{k},z_1)\mathbf{f}(z_1)\mathbf{j}^{(1)}(\mathbf{k}), \quad \mathbf{j}^{(1)}(\mathbf{k})\mathbf{f}(z_2)\Sigma(\mathbf{k},z_2),$$

$$\Sigma(\mathbf{k},z_1)\mathbf{f}(z_1)\mathbf{j}^{(1)}(\mathbf{k}), \quad \mathbf{j}^{(1)}(\mathbf{k})\mathbf{f}(z_2)\Sigma(\mathbf{k},z_2).$$

Closely related to the above diagrams is a group of diagrams which describe joint fluctuations of one current and two propagators. Two such diagrams labeled (9) and (10) in Fig. 8 can also be expressed in terms of the self-energy:

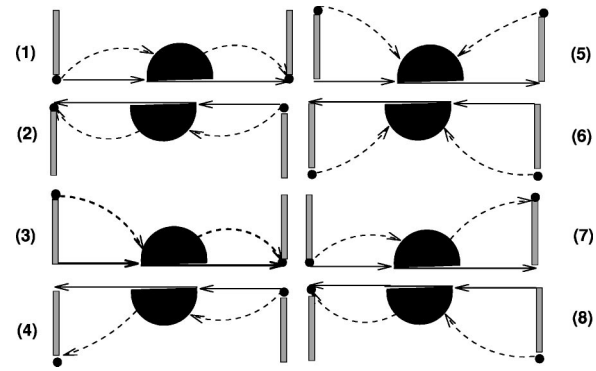

FIG. 9. The scattering diagrams associated with joint fluctuations of the random current terms and one propagator.

$$\Sigma(\mathbf{k},z_2)\mathbf{f}(z_2)\mathbf{j}^{(2)}(\mathbf{k})\mathbf{f}(z_1)\Sigma(\mathbf{k},z_1),$$

$$\Sigma(\mathbf{k},z_1)\mathbf{f}(z_1)\mathbf{j}^{(2)}(\mathbf{k})\mathbf{f}(z_2)\Sigma(\mathbf{k},z_2).$$

If we now gather all the contributions from these diagrams, we may define a renormalized current term as follows:

$$\mathbf{J}^{\text{eff}}(\mathbf{k},z_1,z_2) = \langle\langle \mathbf{j}(\mathbf{k})\rangle\rangle + 2[\Sigma(\mathbf{k},z_2)\mathbf{f}(z_2)\mathbf{j}^{(1)\dagger}(\mathbf{k}) + \mathbf{j}^{(1)\dagger}(\mathbf{k})\mathbf{f}(z_1)\Sigma(\mathbf{k},z_1)] + \Sigma(\mathbf{k},z_2)\mathbf{f}(z_2)\mathbf{j}^{(2)}(\mathbf{k})\mathbf{f}(z_1)\Sigma(\mathbf{k},z_1). \tag{18}$$

The contribution of these disorder-renormalized currents and propagators to the correlation function is

$$\langle\langle \mathcal{S}_{(1)}(z_1,z_2)\rangle\rangle = \int_{\text{BZ}} \frac{d^3\mathbf{k}}{8\pi^3}\text{Tr}[\mathbf{J}^{\text{eff}}(\mathbf{k},z_1,z_2)\langle\langle \mathbf{G}^v(\mathbf{k},z_1)\rangle\rangle\mathbf{J}^{\text{eff}}(\mathbf{k},z_1,z_2)^\dagger\langle\langle \mathbf{G}^c(\mathbf{k},z_2)\rangle\rangle]. \tag{19}$$

We now turn to terms which involve joint fluctuations between the two current terms and one propagator. We shall show that the corrections due to these terms are also related to the self-energy. Such diagrams are shown in Fig. 9. Contribution of these diagrams is given by

$$\langle\langle \mathcal{S}_{(2)}(z_1,z_2)\rangle\rangle = 4\int_{\text{BZ}} \frac{d^3\mathbf{k}}{8\pi^3}\text{Tr}[\mathbf{j}^{(1)}(\mathbf{k})\mathbf{f}(z_1)\Sigma(\mathbf{k},z_1)\mathbf{f}(z_1)\mathbf{j}^{(1)\dagger}(\mathbf{k})\langle\langle \mathbf{G}(\mathbf{k},z_2)\rangle\rangle + \mathbf{j}^{(1)\dagger}(\mathbf{k})\mathbf{f}(z_2)\Sigma(\mathbf{k},z_2)\mathbf{f}(z_2)\mathbf{j}^{(1)}(\mathbf{k})\langle\langle \mathbf{G}(\mathbf{k},z_1)\rangle\rangle]. \tag{20}$$

These terms have a slightly different structure than those shown in Fig. 7. However, they still depend only on the self-energy.

Intuitively, we expect these to be the dominant disorder scattering correction to the averaged current. It is important to note that this correction can be obtained from the self-energy and is therefore eminently computationally feasible in the case of realistic alloys, once we have a feasible method for obtaining the self-energy.

There are other scattering diagrams which are not related to the self-energy, but rather to the vertex corrections. In these diagrams, a disorder line connects both the electron propagators directly. We expect these corrections to be less dominant. For the sake of completeness, we shall indicate how to obtain them in the Appendix. We should note that since these corrections are related to the vertex corrections and we shall indicate how to obtain them within a ladder approximation, we need not sacrifice these terms in a calculation for a realistic alloy if we do not wish to do so. However, in most cases we expect their contribution to be relatively small.

B. The vertex correction

We shall now examine the scattering diagrams we have left out, namely those in which disorder lines connect both the propagators directly. These lead to vertex corrections due to electron-electron and electron-hole correlated propagation. Figure 10 shows a few of these diagrams. In general, we obtain a Bethe-Salpeter equation for the averaged two-particle propagator. We shall consider only one special class of vertex diagrams in this paper, namely the scattering dia-

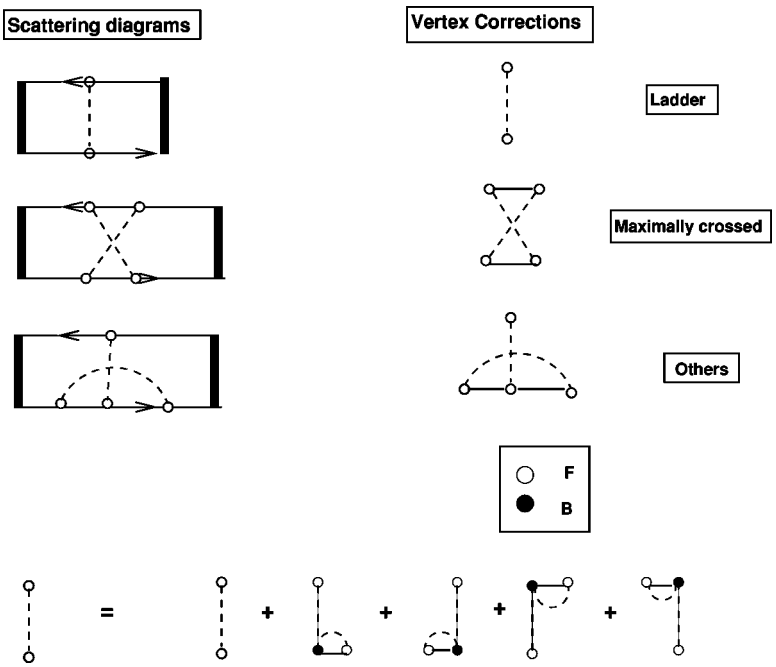

FIG. 10. The scattering diagrams leading to vertex corrections.

grams which are built out of repeated vertices shown on the first line of Fig. 10. These are called the ladder diagrams and can be summed up to all orders. This is the disorder scattering version of the random-phase approximation (RPA) for electron-electron scattering. There is another form of diagrams shown on the second line of Fig. 10 with ladder insertions between the crossed vertices. These are known as maximally crossed diagrams. These diagrams lead to the localization effect.

Here we shall sum the ladder diagrams to all orders. The contribution of the ladder diagram shown as the second diagram on the top line in Fig. 11 is

$$\sum_{R_1R_2R_3R_4}\sum_{R_5}\sum_{L_1L_2L_3L_4L_5L_6}\mathbf{J}^{\mathrm{eff}}_{R_5L_6,R_1L_1}G_{R_1L_1,R_2L_2}(z_1)W^{L_5}_{L_2}G_{R_2L_2,R_3L_3}(z_1)\mathbf{J}^{\mathrm{eff}\dagger}_{R_3L_3,R_4L_4}G_{R_4L_4,R_2L_5}(z_2)G_{R_2L_5,R_5L_6}(z_2),$$

where $G_{RLR'L'}(z)=\langle\langle G^{v/c}_{RLR'L'}(z)\rangle\rangle$ and

$$W^{L}_{L'}=F_L(z_2)\left[\delta_{LL'}+2\sum_{L''}[B_{L''}(z_1)G_{RL'',RL'}(z_1)+B_{L''}(z_2)G_{RL'',RL'}(z_2)]\right]F_{L'}(z_1).$$

Homogeneity in augmented-space means that this is independent of R and it allows us to take the Fourier transforms leading to

$$\left[\int_{\mathrm{BZ}}\frac{d^3\mathbf{k}}{8\pi^3}\mathbf{G}(\mathbf{k},z_2)\mathbf{J}^{\mathrm{eff}}(\mathbf{k},z_1,z_2)\mathbf{G}(\mathbf{k},z_1)\right]\mathbf{W}\left[\int_{\mathrm{BZ}}\frac{d^3\mathbf{k}'}{8\pi^3}\mathbf{G}(\mathbf{k}',z_1)\mathbf{J}^{\mathrm{eff}\dagger}(\mathbf{k}',z_1,z_2)\mathbf{G}(\mathbf{k}',z_2)\right]=\mathbf{\Gamma}(z_1,z_2)\mathbf{W}\hat{\mathbf{\Gamma}}(z_1,z_2). \tag{21}$$

We define

$$\int_{\mathrm{BZ}}\frac{d^3\mathbf{k}}{8\pi^3}\mathbf{G}(\mathbf{k},z_2)\mathbf{J}^{\mathrm{eff}}(\mathbf{k},z_1,z_2)\mathbf{G}(\mathbf{k},z_1)=\mathbf{\Gamma}(z_1,z_2),$$

$$\int_{\mathrm{BZ}}\frac{d^3\mathbf{k}'}{8\pi^3}\mathbf{G}(\mathbf{k}',z_1)\mathbf{J}^{\mathrm{eff}}(\mathbf{k}',z_1,z_2)^{\dagger}\mathbf{G}(\mathbf{k}',z_2)=\hat{\mathbf{\Gamma}}(z_1,z_2).$$

Let us now look at the contribution of the set of ladder diagrams. Each one of them has the same structure as Eq. (21). We may then sum up the series as follows.

Let us define

$$\lambda^{L_1L_2}_{L_3L_4}(z_1,z_2)=\int_{\mathrm{BZ}}\frac{d^3\mathbf{k}}{8\pi^3}G_{L_3L_4}(\mathbf{k},z_1)G_{L_2L_1}(\mathbf{k},z_2),$$

$$\omega^{L_1L_2}_{L_3L_4}=W^{L_1}_{L_3}\delta_{L_1L_2}\delta_{L_3L_4}.$$

These supermatrices in $\{L\}$ space are written as $\underline{\underline{\lambda}}$ and $\underline{\underline{\omega}}$. The full ladder vertex may now be written as

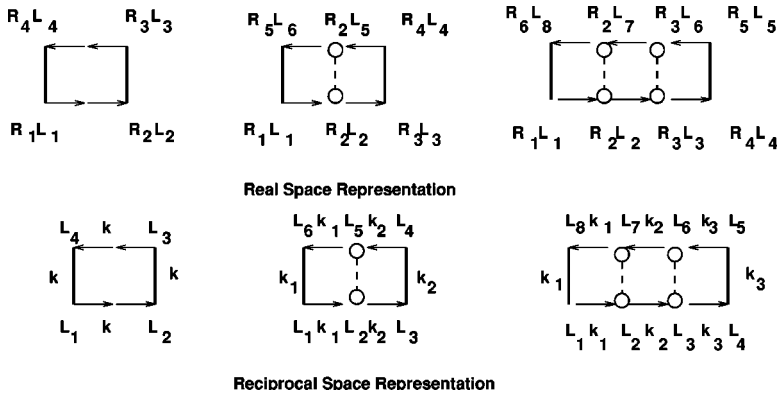

FIG. 11. The ladder scattering diagrams for the vertex correction in real-space and reciprocal-space representations.

$$\underline{\underline{\Lambda}}(z_1,z_2) = \underline{\underline{\omega}} + \underline{\underline{\omega}}\underline{\underline{\lambda}}(z_1,z_2)\underline{\underline{\omega}} + \underline{\underline{\omega}}\underline{\underline{\lambda}}(z_1,z_2)\underline{\underline{\omega}}\underline{\underline{\lambda}}(z_1,z_2)\underline{\underline{\omega}} + \cdots$$
$$= \underline{\underline{\omega}}[\underline{\underline{I}} - \underline{\underline{\lambda}}(z_1,z_2)\underline{\underline{\omega}}]^{-1}. \tag{22}$$

The ladder diagram vertex correction now can be written as

$$\langle\langle S_{\text{ladder}}(z_1,z_2)\rangle\rangle = \text{Tr}\sum_{L_1L_2L_3L_4}\sum \Gamma^{L_1}_{L_2}(z_1,z_2)\Lambda^{L_1L_3}_{L_2L_4}\hat{\Gamma}^{L_3}_{L_4}(z_1,z_2)$$
$$= \text{Tr}\mathbf{\Gamma}(z_1,z_2)\otimes\hat{\mathbf{\Gamma}}(z_1,z_2)\Lambda(z_1,z_2). \tag{23}$$

VI. COMMENTS AND CONCLUSION

Starting from the pseudo-fermion picture in the augmented-space method, we have obtained an expression for the configuration-averaged optical conductivity. The disorder scattering renormalizes both the electron propagators as well as the current terms. We have shown that the dominant corrections to the averaged current can be related to the self-energy. For the sake of completeness, we have also shown that the remaining correction terms are related to the vertex corrections. We have also indicated how to obtain the vertex corrections within the ladder approximation. Once we set up a computationally feasible technique for the computation of the self-energy and the ladder approximation to the vertex correction, all the correction terms can be easily obtained. In an earlier communication,[30] we have suggested the augmented-space recursion as a feasible technique for obtaining $\Sigma(\mathbf{k})$ and have applied it for obtaining the complex band structure and density of states of a series of realistic metallic alloys, namely AgPd and AuFe and most recently NiPt among others. We propose to use that technique and the results derived here to obtain the configuration-averaged optical conductivity in disordered metallic alloys. We intend to study, through numerical calculations, the relative importance of the contribution of the different correction terms.

APPENDIX: CORRECTIONS TO THE CURRENT TERM RELATED TO THE VERTEX CORRECTIONS

For the sake of completeness, we shall also indicate the contribution of those scattering diagrams to the current which cannot be directly related to the self-energy but rather to vertex corrections.

These remaining diagrams are shown in the left column of Fig. 12. These diagrams cannot be related to the self-energies, but rather to specific vertex correction diagrams between the two propagators. There are three categories of diagrams: ones that involve $\tilde{\mathbf{F}}$ vertices [labeled (11)–(13)], ones that involve $\tilde{\mathbf{B}}$ [labeled (14)–(16)] -type vertices, and those that involve both [labeled (17)–(18)].

The first category of diagrams (11)–(13) contributes the following:

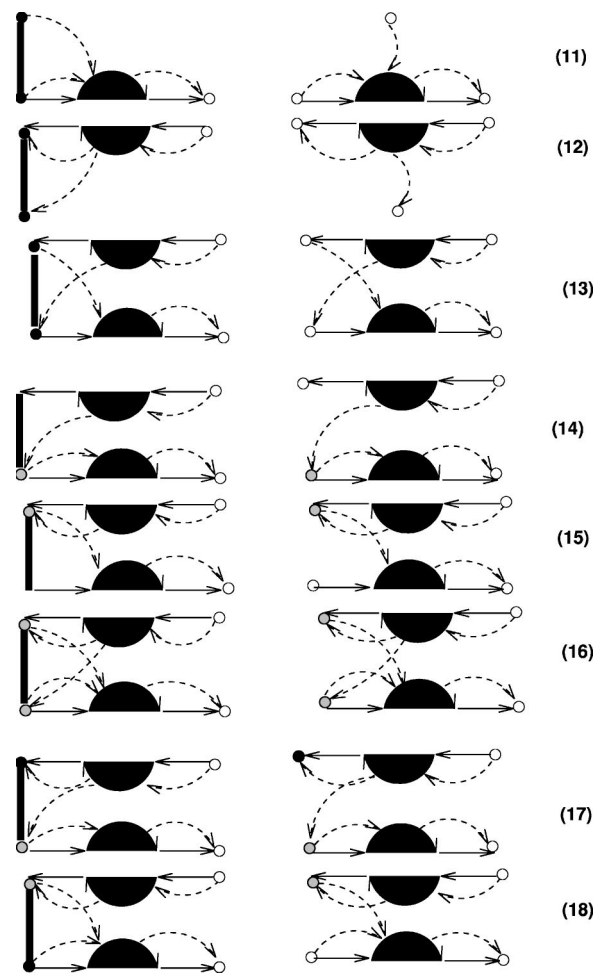

FIG. 12. Renormalized currents (left column) derived from vertex corrections (right column).

$$\tilde{\mathbf{F}}(z_1)\mathbf{F}^{-1}(z_1)\mathbf{j}^{(2)}(\mathbf{k})\tilde{\mathbf{F}}(z_2)\mathbf{F}^{-1}(z_2)\Lambda^{(F)}(\mathbf{0},\mathbf{k};z_1,z_2) \Rightarrow \text{diagram (11)},$$

$$\tilde{\mathbf{F}}(z_1)\mathbf{F}^{-1}(z_1)\mathbf{j}^{(2)}(\mathbf{k})\tilde{\mathbf{F}}(z_2)\mathbf{F}^{-1}(z_2)\Lambda^{(F)}(\mathbf{k},\mathbf{0};z_1,z_2) \Rightarrow \text{diagram (12)},$$

$$\tilde{\mathbf{F}}(z_1)\mathbf{F}^{-1}(z_1)\mathbf{j}^{(2)}(\mathbf{k})\tilde{\mathbf{F}}(z_2)\mathbf{F}^{-1}(z_2)\Lambda^{(F)}(\mathbf{k},\mathbf{k};z_1,z_2) \Rightarrow \text{diagram (13)}.$$

Inserting the expressions for $\mathbf{F}(z)$ and $\tilde{\mathbf{F}}$, we get a total contribution,

$$\mathbf{J}_1 = \mathbf{f}(z_1)\mathbf{j}^{(2)}(\mathbf{k})\mathbf{f}(z_2)\{\Lambda^{(F)}(\mathbf{0},\mathbf{k},z_1,z_2) + \Lambda^{(F)}(\mathbf{k},\mathbf{0},z_1,z_2) + \Lambda^{(F)}(\mathbf{k},\mathbf{k},z_2,z_1)\}. \tag{A1}$$

Here, the vertex correction term $\Lambda^{(F)}$ involves only F-like vertices in all four legs. Similarly, for the other two sets of diagrams we get

$$\tilde{\mathbf{B}}(z_1)\mathbf{B}^{-1}(z_1)\mathbf{j}^{(1)}(\mathbf{k})\mathbf{F}^{-1}(z_2)\Lambda^{(B)}(\mathbf{k},\mathbf{k};z_1,z_2) \Rightarrow \text{diagram(14)},$$

$$\mathbf{F}^{-1}(z_1)\mathbf{j}^{(2)}(\mathbf{k})\tilde{\mathbf{B}}(z_2)\mathbf{B}^{-1}(z_2)\Lambda^{(B)}(\mathbf{k},\mathbf{k};z_1,z_2) \Rightarrow \text{diagram (15)},$$

$$\tilde{\mathbf{B}}(z_1)\mathbf{B}^{-1}(z_1)\mathbf{j}^{(2)}(\mathbf{k})\tilde{\mathbf{B}}(z_2)\mathbf{B}^{-1}(z_2)\Lambda^{(B)}(\mathbf{k},\mathbf{k};z_1,z_2) \Rightarrow \text{diagram (16)}.$$

The total contribution will be

$$\mathbf{J}_2 = \left\{\frac{2}{\sqrt{x_A x_B}}\mathbf{f}(z_1)\mathbf{j}^{(1)}(\mathbf{k})\mathbf{f}(z_2) + \mathbf{f}(z_1)\mathbf{j}^{(2)}(\mathbf{k})\mathbf{f}(z_2)\right\} \times \Lambda^{(B)}(\mathbf{k},\mathbf{k};z_1,z_2). \tag{A2}$$

$\Lambda^{(B)}$ involves only B-like vertices in its left-hand side legs. Finally, for the last two diagrams,

$$\tilde{\mathbf{B}}(z_1)\mathbf{B}^{-1}(z_1)\mathbf{j}^{(2)}(\mathbf{k})\tilde{\mathbf{F}}(z_2)\mathbf{F}^{-1}(z_2)\Lambda^{(FB)}(\mathbf{k},\mathbf{k};z_1,z_2) \Rightarrow \text{diagram (17)},$$

$$\tilde{\mathbf{F}}(z_1)\mathbf{F}^{-1}(z_1)\mathbf{j}^{(2)}(\mathbf{k})\tilde{\mathbf{B}}(z_2)\mathbf{B}^{-1}(z_2) \times \Lambda^{(FB)}(\mathbf{k},\mathbf{k};z_1,z_2) \Rightarrow \text{diagram (18)}.$$

Their contribution is

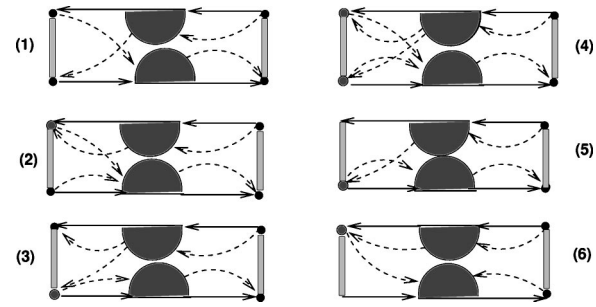

FIG. 13. Some of the scattering diagrams associated with joint fluctuations of the random current terms and two propagators.

$$\mathbf{J}_3 = 2\mathbf{f}(z_1)\mathbf{j}^{(2)}(\mathbf{k})\mathbf{f}(z_2)\Lambda^{(FB)}(\mathbf{k},\mathbf{k};z_1,z_2). \tag{A3}$$

Collecting together terms

$$\Delta\mathbf{J} = \mathbf{J}_1 + \mathbf{J}_2 + \mathbf{J}_3.$$

The contribution of these disorder renormalized currents and propagators to the correlation function is

$$\langle\langle S_{(3)}(z_1,z_2)\rangle\rangle = \int_{\mathrm{BZ}} \frac{d^3\mathbf{k}}{8\pi^3}\mathrm{Tr}[\Delta\mathbf{J}(\mathbf{k},z_1,z_2) \times \langle\langle \mathbf{G}^v(\mathbf{k},z_1)\rangle\rangle \Delta\mathbf{J}(\mathbf{k},z_1,z_2)^\dagger \langle\langle G^c(\mathbf{k},z_2)\rangle\rangle]. \tag{A4}$$

Finally, Fig. 13 shows the diagrams with joint fluctuations of two current terms and two propagators. These are also built out of vertex corrections. Note that each of the six diagrams can be broken up into a left and right part. For the diagrams shown in Fig. 13 all the right parts are the same. Thirty other similar diagrams can be produced by replacing the right part with the five different left parts mirror-imaged. The contribution of these diagrams is then, if

$$\mathbf{K}(\mathbf{k},z_1,z_2) = \mathbf{f}(z_2)\mathbf{j}^{(2)}(\mathbf{k})\mathbf{f}(z_1) + \mathbf{b}(z_2)\mathbf{j}^{(2)}(\mathbf{k})\mathbf{f}(z_1) + \mathbf{f}(z_2)\mathbf{j}^{(2)}(\mathbf{k})\mathbf{b}(z_1) + \mathbf{b}(z_2)\mathbf{j}^{(2)}(\mathbf{k})\mathbf{b}(z_1),$$

where

$$\mathbf{b}(z) = \frac{x_B - x_A}{\sqrt{x_A x_B}}\mathbf{f}(z),$$

$$\langle\langle \mathcal{S}_{(4)}(z_1,z_2)\rangle\rangle = \int_{\mathrm{BZ}} \frac{d^3\mathbf{k}}{8\pi^3}\mathrm{Tr}\mathbf{K}(\mathbf{k},z_1,z_2) \otimes \mathbf{K}^\dagger(\mathbf{k},z_1,z_2)\Lambda(\mathbf{k},\mathbf{k},z_1,z_2). \tag{A5}$$

*Electronic address: kamal@bose.res.in

[1] O. K. Andersen, Phys. Rev. B **12**, 3060 (1975).
[2] O. Jepsen and O. K. Andersen, Solid State Commun. **9**, 1763 (1971).
[3] A. Mookerjee, J. Phys. C **6**, 1340 (1973).
[4] T. Kaplan and L. J. Gray, Phys. Rev. B **15**, 3260 (1977).
[5] T. Saha, I. Dasgupta, and A. Mookerjee, J. Phys.: Condens. Matter **8**, 1979 (1996).
[6] I. Dasgupta, T. Saha, and A. Mookerjee, J. Phys.: Condens. Matter **9**, 3529 (1997).

[7] S. Ghosh, N. Das, and A. Mookerjee, Int. J. Mod. Phys. B **21**, 723 (1999).
[8] J. M. Ziman, Philos. Mag. **6**, 1013 (1961).
[9] C. C. Bradley, T. E. Faber, E. G. Wilson, and J. M. Ziman, Philos. Mag. **7**, 865 (1962).
[10] T. E. Faber and J. M. Ziman, Philos. Mag. **11**, 153 (1965).
[11] R. Evans, D. A. Greenwood, and P. Lloyd, Phys. Lett. **35A**, 57 (1980).
[12] L. Roth and V. A. Singh, J. Phys. (Paris), Colloq. **C8**, 459 (1980).
[13] L. Roth, Phys. Rev. B **9**, 2476 (1974).
[14] V. A. Singh and L. Roth, Bull. Am. Phys. Soc. **25**, 242 (1980).
[15] S. Asano and F. Yonezawa, J. Phys. F: Met. Phys. **10**, 75 (1980).
[16] B. Velický, Phys. Rev. **184**, 614 (1969).
[17] F. Brouers and A. V. Vedyayev, Phys. Rev. B **5**, 348 (1972).
[18] K. Niizeki, J. Phys. C **10**, 211 (1977); **10**, 2131 (1977); **10**, 2141 (1977).
[19] K. Hoshino and M. Watabe, J. Phys. Soc. Jpn. **43**, 583 (1977).
[20] K. Niizeki and K. Hoshino, J. Phys. C **10**, 3351 (1977).
[21] A. Mookerjee, J. Phys. C **9**, 1225 (1976).
[22] P. L. Leath, Phys. Rev. B **2**, 3078 (1970).
[23] R. Harris and M. Plischke, Solid State Commun. **11**, 1165 (1972).
[24] M. Nauciel-Bloch and R. Riedinger, J. Phys. F: Met. Phys. **4**, 1032 (1974).
[25] A. Mookerjee, J. Phys. C **8**, 1524 (1975).
[26] A. Mookerjee, P. K. Thakur, and M. Yussouff, J. Phys. C **18**, 4677 (1985).
[27] A. Mookerjee and P. K. Thakur, J. Phys. C **21**, 943 (1988).
[28] T. D. Schultz and D. Shapero, Phys. Rev. B **7**, 5090 (1973).
[29] P. Biswas, B. Sanyal, M. Fakhruddin, A. Halder, A. Mookerjee, and M. Ahmed, Int. J. Mod. Phys. B **11**, 3703 (1997).
[30] K. K. Saha and A. Mookerjee, cond-mat/0405175 (unpublished); P. Biswas, B. Sanyal, M. Fakhruddin, A. Halder, A. Mookerjee, and M. Ahmed, J. Phys.: Condens. Matter **7**, 8569 (1995).
[31] This statement has to be modified in some situations, like localized states in band tails, where unlikely configurations play an important role and configuration averaging is not meaningful.
[32] These spins denote configurations rather than electron spins.
[33] A nonseparable diagram cannot be broken into two along an electron line without also breaking a pseudo-fermion line.